Charged defects and phonon Hall effects in ionic crystals

B. Flebus[1] and A. H. MacDonald[2]

[1]*Department of Physics, Boston College, 140 Commonwealth Avenue, Chestnut Hill, Massachusetts 02467, USA*
[2]*Physics Department, University of Texas, Austin, Texas 78712, USA*

It has been known for decades that a magnetic field can deflect phonons as they flow in response to a thermal gradient, producing a thermal Hall effect. Several recent experiments have revealed ratios of the phonon Hall conductivity κ_H to the phonon longitudinal conductivity κ_L in oxide dielectrics that are larger than 10^{-3} when phonon mean-free paths exceed phonon wavelengths. At the same time κ_H/κ_L is not strongly temperature dependent. We argue that these two properties together imply a mechanism related to phonon scattering from defects that break time-reversal symmetry, and we show that Lorentz forces acting on charged defects can produce substantial skew-scattering amplitudes and related thermal Hall effects.

Introduction. In recent years the thermal Hall effect has frequently been employed as an informative probe of strongly correlated materials [1–20]. In the process, it has become clear that relatively large thermal Hall conductivities (κ_H) that are linearly proportional to magnetic field B are common in oxide dielectrics. The linear dependence of κ_H on B is expected since this nonreciprocal transport coefficient requires time-reversal symmetry breaking. What is surprising is not that $\kappa_H/B \neq 0$, but that it is relatively large. For magnetic fields ~ 10 T, the ratio of κ_H to the longitudinal thermal conductivity κ_L is often larger than 10^{-3} over a wide range of temperatures [1–4].

Large thermal Hall conductivities are not limited to magnetic materials, and even in magnetic materials usually have an onset that is not related to that of magnetic order [1]. In La_2CuO_4 the thermal Hall conductivity is almost isotropic [3], like the phonon spectrum, whereas the magnon spectrum is quasi-two-dimensional. Although there must be a magnon Hall effect, whose theoretical description is of interest [21–25], it is therefore not typically the dominant source of the thermal Hall effect. Phonons, the dominant heat carriers in most dielectrics, must also have a Hall effect [12].

Large thermal Hall effects are normally observed in a temperature range over which the the phonon mean-free path ℓ exceeds the typical wavelength of thermally active phonons, $\lambda_T \sim \hbar c/k_B T$, where c is the mode velocity. When this condition is satisfied, phonon transport can be described using a Boltzmann equation, and the phonon conductivity is limited by phonon scattering. The nonreciprocity could in principle originate from an intrinsic mechanism that acts between scattering events, or from a nonreciprocal property of the extrinsic scatterers. Mechanisms responsible for intrinsic chirality in phonon transport have been extensively investigated [6–8,12,26,27]. Coupling to a spin environment can, for example, provide phonon bands with a finite Hall viscosity, η_H [19,20], which characterizes the strength of the time-reversal symmetry breaking inherited from the spin system. Magnetic

fields also influence the lattice dynamics of ionic crystals directly through the Lorentz forces that act on moving ions [28]. The Lorentz force couples longitudinal in-phase motion of the cations and anions to out-of-phase transverse motion. At small k the chiral components of acoustic phonon polarization vectors vanish like $(ka)^2$. It follows that η_H has a Lorentz force
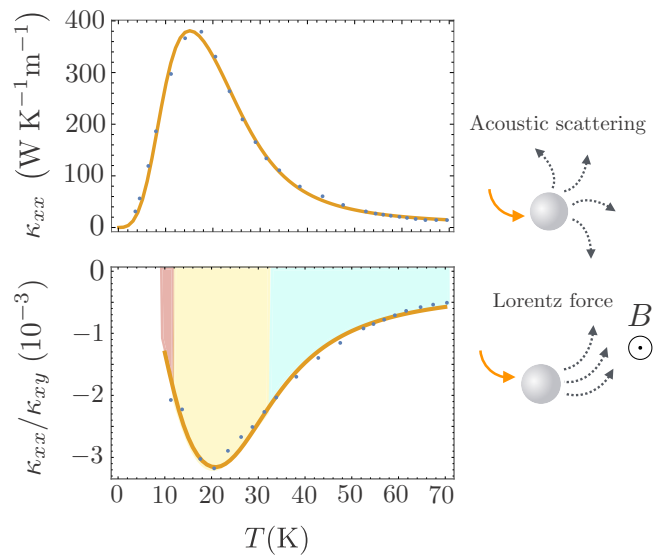

FIG. 1. Left side: Longitudinal thermal conductivity κ_{xx} (top panel) and the thermal Hall to longitudinal conductivity ratio κ_{xy}/κ_{xx} (bottom panel) of a model in which scattering off charge defects is weakly nonreciprocal in the presence of a magnetic field. Right side: Schematic illustration of scattering of acoustic waves on charged defects. Parameters have been chosen to fit the data (blue dots) reported in Ref. [15]. The yellow, blue, and red shading in the bottom panel identifies the temperature ranges in which boundary, defect, and umklapp scattering are respectively dominant. Similarly high-quality fits can be achieved in all systems that we have examined.

contribution $\sim Z^* eB/(ca) = M\Omega_{cI}/a$, where $\omega_{cI} = Z^* eB/Mc$ is the ion cyclotron frequency, Z^* is the effective ion charge, M is the ion mass, and a is the crystal lattice constant. Whatever its origin, Hall viscosity combined with nonchiral phonon scattering always produces a thermal Hall conductivity. Because the chirality of the active phonons is proportional to k^2, and the typical $k \sim \lambda_T^{-1} \propto T$, this mechanism always yields a κ_H/κ_L ratio that declines with decreasing temperature. (Guo *et al.* have recently concluded that the intrinsic mechanism yields $\kappa_H/\kappa_L \sim T^4$ [20] behavior.) Experimentally κ_H/κ_L is weakly temperature dependent except at the lowest temperatures where boundary scattering starts to play a role, pointing to an extrinsic mechanism. In order to retain its impact at low temperatures, time-reversal symmetry breaking must be embedded in the properties of the phonon scatterers, not the phonon medium.

Our model for phonon Hall effects applies when the phonon mean-free path ℓ exceeds the thermal wavelength λ_T of acoustic phonons with energy $\hbar\omega \sim k_B T$, i.e., $\ell \gg \lambda_T$. The mean-free path can be estimated from measured thermal conductivities and heat capacities using the relationship $\ell \sim \kappa/cC$, where C is the heat capacity. The thermal wavelength is of order $\sim a T_D/T$, where T_D is the acoustic phonon Debye temperature, and a is the crystal lattice constant. It has been understood for decades [29–31] that phonon transport in this regime, which is commonly attained in good crystals, can be described using a Boltzmann equation. In the temperature range of interest, scattering of long-wavelength longitudinal acoustic (LA) phonons by defects, for example oxygen vacancies, limits thermal transport [31]. The removal or the addition of an atom from a lattice site disrupts the local bonding, yielding strain fields that produce a crudely spherical defect with elastic properties that differ from those of the surrounding medium, as depicted in Fig. 1. Since oxygen vacancies and interstitials are dopants, the ions in its neighborhood have a net charge when the donor bound electronic levels are not occupied, and will therefore experience a local Lorentz force. In this Letter we propose that the thermal Hall effect in many oxide dielectrics is due to nonreciprocal phonon scattering from charged defects. Specifically, we show that a contribution to phonon skew scattering that is linear in magnetic field results from interference between Lorentz force and acoustic potential scattering processes. As illustrated in Fig. 1, this physical picture is able to account for many observations.

Phonon Boltzmann equation. We consider the steady-state phonon distribution function $f_{\mathbf{k},s}$ of a system driven from equilibrium by a temperature gradient ∇T. (Here $\mathbf{k}$ is the phonon wave vector and s the mode label.) We write $f_{\mathbf{k},s} = f_{\mathbf{k},s}^{(0)} + g_{\mathbf{k},s}$, where $f_{\mathbf{k},s}^{(0)}$ is the equilibrium Bose-Einstein distribution function and $g_{\mathbf{k}s}$ is linear in ∇T. At low temperatures the thermal conductivity is limited by elastic scattering of longitudinal phonons [30,31]. The Boltzmann equation therefore reads

$$\omega_{\mathbf{k}} \frac{\partial \omega_{\mathbf{k}}}{\partial \mathbf{k}} \cdot \left(\frac{\nabla T}{T} \right) \left(-\frac{\partial f_{\mathbf{k}}^{(0)}}{\partial \omega_{\mathbf{k}}} \right) = \sum_{\mathbf{q}} (W_{\mathbf{q}\to\mathbf{k}} \, g_{\mathbf{q}} - W_{\mathbf{k}\to\mathbf{q}} \, g_{\mathbf{k}}), \tag{1}$$

where we have restricted attention to the longitudinal phonon mode with frequency $\omega_{\mathbf{k}}$. Here, $W_{\mathbf{k}\to\mathbf{q}}$ is the rate of elas-

tic scattering from initial state ($\mathbf{k}$) to final state ($\mathbf{q}$). For temperatures well below the Debye temperature, the phonon Hall conductivity is largest, $\omega_{\mathbf{k}} \approx c|\mathbf{k}|$, where c is the longitudinal phonon velocity. Nonreciprocal (skew) phonon scattering ($W_{\mathbf{q}\to\mathbf{k}} \neq W_{\mathbf{k}\to\mathbf{q}}$) requires broken time-reversal symmetry that is, in the case of interest, supplied by an external magnetic field $\mathbf{B} = B\hat{\mathbf{n}}_B$, where $\hat{\mathbf{n}}_B$ is a unit vector along the direction of the field. For a cubic crystal with short-range scatterers,

$$W_{\mathbf{k}\to\mathbf{q}} = \frac{1}{V} \tau_\omega^{-1} \nu_\omega^{-1} [1 - \Lambda_\omega \hat{\mathbf{n}}_B \cdot (\hat{\mathbf{k}} \times \hat{\mathbf{q}})] \delta(\omega - cq), \tag{2}$$

where V is the system volume, τ_ω is the phonon relaxation time, ν_ω is the phonon density of states, and $\Lambda_\omega \ll 1$ is a small parameter, calculated explicitly below, that characterizes the ratio of nonreciprocal to reciprocal phonon scattering. When inserted in the Boltzmann equation, Eq. (2) yields the longitudinal (κ_L) and Hall (κ_H) thermal conductivities:

$$\kappa_L = \frac{k_B^4 T^3}{2\pi^2 \hbar^3 c} \int dx \, \tau_\omega \frac{x^4 e^x}{(e^x - 1)^2}, \tag{3}$$

$$\kappa_H = \frac{k_B^4 T^3}{2\pi^2 \hbar^3 c} \int dx \, \frac{\Lambda_\omega \tau_\omega}{3} \frac{x^4 e^x}{(e^x - 1)^2}, \tag{4}$$

with $\hbar\omega = k_B T x$. It follows that $\kappa_H/\kappa_L \sim \Lambda_\omega$ at $\omega \sim k_B T$. The goal of the next section is to estimate the parameter Λ_ω by investigating the interference between conventional long-wavelength acoustic and Lorentz scattering processes.

Low-temperature phonon scattering. Since the ions in the vicinity of a dopant complex have a net charge, the local Lorentz force does not vanish in the interior of the scattering center, as sketched in Fig. 1. Below we show that a contribution to phonon skew scattering that is linear in magnetic field results from the interference between this Lorentz force and the acoustic scattering potential. The strength of the effect can be characterized by the ion-cyclotron frequency ω_c, which is $\sim 10^5$ Hz at $B = 10$ T, depending on the ion charge and mass.

In order to obtain an explicit form for the scattering amplitude we first examine acoustic scattering in the absence of a magnetic field. It is convenient to rewrite the acoustic wave equation in this limit as

$$\left(\nabla^2 + K_n^2 \right) \mathbf{u}_n(\mathbf{r}) - \left(1 - \frac{K_n^2}{k_n^2} \right) \nabla [\nabla \cdot \mathbf{u}_n(\mathbf{r})] = 0, \tag{5}$$

where $K_n = \omega/c_{Tn}$ and $k_n = \omega/c_{Ln}$, where $n = 1$ (2) labels the region outside (inside) the defect. Here $c_{Tn}^2 = \mu_n/\rho_n$ and $c_{Ln}^2 = (\lambda_n + 2\mu_n)/\rho_n$ are, respectively, the squares of the transverse and longitudinal phonon velocities, ρ_n is the mass density, and λ_n and μ_n are Lamé constants. It is known that ionic compounds, including high-T_c superconductors, display acoustic wave attenuation [32–36] that survives to $T = 0$. Several experimental studies have observed a correlation between acoustic wave attenuation and the density of oxygen defects [35–37]. Inelastic relaxation effects in solids can appear, for example, where the strain fields of the probing elastic wave differentially alter the energies of the atomic sites available to mobile species [38]. We account for these small absorption losses by including a kinetic viscosity coefficient $\eta_{1(2)}\omega \ll \lambda_{1(2)}, \mu_{1(2)}$ [39] in the acoustic model of the

homogeneous and defect region, letting

$$\mu_{1(2)} \to \mu_{1(2)} - i\eta_{1(2)}\omega,$$
$$\lambda_{1(2)} \to \lambda_{1(2)} - i\eta_{1(2)}\omega. \quad (6)$$

When a longitudinal wave propagating in the z direction ($\mathbf{k} = k\hat{\mathbf{z}}$ [40]) impinges on the surface of the spherical scatterer, it can be scattered either as a longitudinal wave or as a transverse wave. The scattering problem (5) can be conveniently solved in spherical coordinates by introducing the scalar functions π_{Ln} and π_{Tn} defined by [41–47]

$$\mathbf{u}_{\mathrm{Ln}} = -\frac{1}{k_n^2}\nabla \pi_{Ln},$$
$$\mathbf{u}_{\mathrm{Tn}} = \frac{1}{K_n}\nabla \times \nabla \times (\mathbf{r}\pi_{Tn}). \quad (7)$$

The scalar potentials corresponding to incident (^{i}), transmitted (^{t}), and scattered (^{s}) waves can be written as [46]

$$r\pi_L^i = \sum_{l=0}^{\infty} i^{l+1}(2l+1)\psi_l(k_1 r)P_l(\cos\theta), \quad (8)$$

$$r\pi_L^t = \sum_{l=0}^{\infty} i^{l+1}A_l(2l+1)\psi_l(k_2 r)P_l(\cos\theta), \quad (9)$$

$$r\pi_T^t = \frac{1}{K_2}\sum_{l=1}^{\infty} i^{l+1}B_l(2l+1)\psi_l(K_2 r)P_l(\cos\theta), \quad (10)$$

$$r\pi_L^s = \sum_{l=0}^{\infty} i^{l+1}C_l(2l+1)\zeta_l(k_1 r)P_l(\cos\theta), \quad (11)$$

$$r\pi_T^s = \frac{1}{K_1}\sum_{l=1}^{\infty} i^{l+1}D_l(2l+1)\zeta_l(K_1 r)P_l(\cos\theta), \quad (12)$$

with

$$\psi_l(x) = \sqrt{x\pi/2}J_{l+1/2}(x),$$
$$\zeta_l(x) = \sqrt{x\pi/2}H_{l+1/2}^{(1)}(x), \quad (13)$$

where $J_{l+1/2}(x)$ and $H_l^{(1)}(x)$ are the half-order cylindrical Bessel and Hankel functions, $P_l(\cos\theta)$ is the Legendre function of degree l, and θ is the scattering angle. The coefficients A_l, B_l, C_l, and D_l are obtained by imposing the continuity of the displacement field and the stress tensor at the boundary radius $r = a$:

$$u_{r(\theta)}^t = u_{r(\theta)}^i + u_{r(\theta)}^s, \qquad \sigma_{rr(r\theta)}^t = \sigma_{rr(r\theta)}^i + \sigma_{rr(r\theta)}^s, \quad (14)$$

where the stress tensor components

$$\sigma_{rr} = \lambda \nabla \cdot \mathbf{u} + 2\mu \partial_r u_r, \quad (15)$$

$$\sigma_{r\theta} = \mu\left(\partial_r u_\theta - \frac{u_\theta}{r} + \frac{1}{r}\partial_\theta u_r\right). \quad (16)$$

If the difference in mass density and Lamé constants between the two regions is small, i.e., ρ_1/ρ_2, μ_1/μ_2, $\lambda_1/\lambda_2 \sim 1$, one can safely neglect wave interconversion, i.e., $D_l \ll C_l$ for each l. Thus, most of the incident longitudinal acoustic wave amplitude will be scattered as a longitudinal wave. In the Rayleigh scattering regime [48], the wavelength of acoustic waves is much larger than the defect size, i.e., $ka \ll 1$. To leading order

in ka the scattered wave is dominated by its $l = 0$ component

$$\mathbf{u}_{\mathbf{k}'L}(\mathbf{r}) = \hat{\mathbf{e}}_L \frac{e^{ikr}}{r}f_{\mathbf{k}L\to\mathbf{k}'L}, \quad (17)$$

where $\hat{\mathbf{e}}_L = (\cos\phi\sin\theta, \sin\phi\sin\theta, \cos\theta)$ and $\mathbf{k}' = k\hat{\mathbf{e}}_L$ are, respectively, the polarization and the wave vector of the outgoing LA wave. Here $f_{\mathbf{k}L\to\mathbf{k}'L}$ is the longitudinal scattering amplitude from $\mathbf{k}$ to $\mathbf{k}'$:

$$f_{\mathbf{k}L\to\mathbf{k}'L} = \frac{\mathrm{Im}C_0 - i\mathrm{Re}C_0}{k}, \quad (18)$$

with $(\mathrm{Im}C_0)^2 + (\mathrm{Re}C_0)^2 = -\mathrm{Re}C_0$, as dictated by the extinction theorem [49]. Retaining only terms linear in the small parameters $\eta_{1(2)}\omega/\mu_{1(2)}$, we find

$$\mathrm{Im}C_0 \simeq +i\frac{(ka)^3}{3}\frac{3(\lambda_1 - \lambda_2) + 2(\mu_1 - \mu_2)}{3\lambda_2 + 2(2\mu_1 + \mu_2)}, \quad (19)$$

$$\mathrm{Re}C_0 \simeq +\frac{\eta_1\omega(4\mu_1 + 6\mu_2 + 9\lambda_2 - 4\lambda_1)}{(3\lambda_2 + 4\mu_1 + 2\mu_2)^2}(ka)^3$$
$$-\frac{5\eta_2\omega(\lambda_1 + 2\mu_1)}{(3\lambda_2 + 4\mu_1 + 2\mu_2)^2}(ka)^3. \quad (20)$$

Interference between Rayleigh and Lorentz scattering. Working in the continuum elasticity theory limit valid at low temperatures, we describe the phonons by a displacement vector field $\mathbf{u}(\mathbf{r})$ that satisfies the following wave equation:

$$\sum_{j=x,y,z}\left[A_{ij}^0 + A_{ij}^R + A_{ij}^L - \omega^2\delta_{ij}\right]u_j(\mathbf{r}) = 0, \quad (21)$$

where A_{ij}^0 is the acoustic differential operator in the absence of a magnetic field, A_{ij}^R is the difference between the acoustic differential operator inside and outside the defect region, accounted for in the previous section, and A^L is a Lorentz force term that acts only inside the defect. For a uniform isotropic medium

$$A^0 = \begin{pmatrix} c_1^2 k_x^2 + c_{T1}^2 k^2 & c_1^2 k_x k_y & c_{L1}^2 k_x k_z \\ c_1^2 k_x k_y & c_{T1}^2 k^2 + c_1^2 k_y^2 & c_1^2 k_y k_z \\ c_1^2 k_x k_z & c_1^2 k_y k_z & c_1^2 k_z^2 + c_{T1}^2 k^2 \end{pmatrix}, \quad (22)$$

where $k_i = -i\nabla_i$, $k^2 = k_x^2 + k_y^2 + k_z^2$, and $c_1^2 = c_{L1}^2 - c_{T1}^2$. For a given frequency ω, there are three independent solutions of unperturbed elastic waves with vector displacement fields $\mathbf{u}_{\mathbf{k}\alpha}(\mathbf{r}) = \hat{\mathbf{e}}_\alpha\cos(\mathbf{k}\cdot\mathbf{r})$, where $|\mathbf{k}| = \omega/c_{L1}$ for the longitudinal mode ($\mathbf{k}\times\hat{\mathbf{e}}_{L1} = 0$) and $|\mathbf{k}| = \omega/c_{T1}$ for two degenerate transverse ($\mathbf{k}\cdot\hat{\mathbf{e}}_\alpha = 0$) modes.

The ions that surround a charged defect are subject to a Lorentz force that is perpendicular to the applied magnetic field and to the ion velocity. Our goal is to calculate the corrections to the phonon scattering rate that are linear in Lorentz force, and hence in magnetic field. This correction is guaranteed by time-reversal symmetry to be nonreciprocal. The Lorentz force contribution to the acoustic differential operator,

$$A_{ij}^L = i\omega\omega_c(\hat{\mathbf{j}}\times\hat{\mathbf{i}})\cdot\mathbf{n}_B, \quad (23)$$

is nonzero inside the defect sphere. Here $\omega_c = \rho_c B/\rho_2$ is the effective ion cyclotron frequency and ρ_c is the charge density of the defect region.

The scattering rate from an incoming longitudinal wave with wave vector $\mathbf{k}$ to an outgoing unperturbed wave with wave vector $\mathbf{k}'$ is related to the acoustic scattering T matrix by

$$W_{\mathbf{k}\to\mathbf{k}'} = \frac{2\pi}{V^2\omega^2}\,|\langle\mathbf{k}'|T|\mathbf{k}\rangle|^2\delta(\omega_{\mathbf{k}'}-\omega), \qquad (24)$$

where $T = (A^R + A^L) + (A^R + A^L)G^0T$ is the total acoustic scattering T matrix and

$$G^0 = \left[\delta_{ij}\,(\omega+i\eta)^2 - A^0_{ij}\right]^{-1} \qquad (25)$$

is the unperturbed acoustic Green's function. To first order in A^L, $T = T^R + T^R(A^R)^{-1}A^L(A^R)^{-1}T^R + \cdots$ [50], where $T^R = A^R + A^RG^0T^R$ is the Rayleigh scattering T matrix, which is related to the scattering amplitude calculated above by

$$f_{\mathbf{k}L\to\mathbf{k}'L} = -\frac{1}{4\pi}\frac{1}{c^2_{L1}}\langle\mathbf{k}', L|T^R|\mathbf{k}, L\rangle. \qquad (26)$$

Because the $B = 0$ long-wavelength phonon scattering is weak, in the long-wavelength Rayleigh limit we can approximate $T^R(A^R)^{-1} \approx I$, which yields $T \approx T^R + A^L$, where

$$\langle\mathbf{k}', L|A^L|\mathbf{k}, L\rangle = i\omega\omega_c(\hat{\mathbf{z}}\times\hat{\mathbf{e}}_L)\cdot\hat{\mathbf{n}}_B$$

$$\times \int d^3\mathbf{r}\,e^{-i(\mathbf{k}'-\mathbf{k})\cdot\mathbf{r}}\Theta(a-r)$$

$$\underbrace{\simeq}_{ka\ll 1} iV_{\text{sp}}\omega\omega_c(\hat{\mathbf{z}}\times\hat{\mathbf{e}}_L)\cdot\hat{\mathbf{n}}_B, \qquad (27)$$

and $\Theta(x)$ is the Heaviside step function and $V_{\text{sp}} = 4\pi a^3/3$ is the defect volume.

Phonon Hall effect. Combining Eqs. (27), (24), (26), and (18), and assuming that the dielectric contains a density n_s of randomly distributed charged defects, we obtain the expression employed below to estimate the phonon Hall effect:

$$W_{\mathbf{k}L\to\mathbf{k}'L} = \frac{2\pi n_s}{V\omega^2}\delta(\omega_{\mathbf{k}'L}-\omega)$$

$$\times\left|4\pi c^2_{L1}\frac{i\text{Re}C_0 - \text{Im}C_0}{k} + iV_{\text{sp}}\omega\omega_c(\hat{\mathbf{z}}\times\hat{\mathbf{e}}_L)\cdot\hat{\mathbf{n}}_B\right|^2. \qquad (28)$$

Random Lorentz forces would on their own yield a phonon scattering rate proportional to B^2, and a skew scattering rate proportional to B^3. The linear in B effect observed experimentally must therefore arise from interference between Rayleigh and Lorentz scattering terms. Retaining only the linear terms and setting $\omega = c_{L1}k$, we obtain an expression for the dimensionless skewness parameter employed in Eq. (4):

$$\Lambda_\omega \simeq \frac{\omega_c\eta_1\left(\frac{4\mu_1}{\lambda_1} + \frac{6\mu_2}{\lambda_1} + \frac{9\lambda_2}{\lambda_1} - 4\right) - 5\omega_c\eta_2\left(1 + \frac{2\mu_1}{\lambda_1}\right)}{\lambda_1\left[\left(1 - \frac{\lambda_2}{\lambda_1}\right) + \frac{2}{3}\left(\frac{\mu_1}{\lambda_1} - \frac{\mu_2}{\lambda_1}\right)\right]^2}. \qquad (29)$$

The right-hand side of Eq. (29) is energy independent, implying that in the Rayleigh scattering regime, the Hall to longitudinal conductivity ratio is temperature independent, with both quantities $\propto T^{-1}$.

We estimate the typical values of Λ_ω at magnetic field $H = 15$ T and temperature $T = 15$ K by setting ω_c to the oxygen

ion cyclotron frequency, with $\rho_c > 0$ for oxygen vacancies [51], and assuming a 1% difference for the Lamé constants inside and outside the defect region with $\lambda_1, \mu_1 > \lambda_2, \mu_2$, $\mu_{1(2)} \sim 0.8\lambda_{1(2)}$ and setting $\eta_2\omega/\lambda_1 > \eta_1\omega/\lambda_1 \sim 10^{-2}$. These estimates yield

$$\frac{\kappa_H}{\kappa_L} \sim -10^{-3}, \qquad (30)$$

which is consistent with the order of magnitude observed in experiment [1–3]. Note that the skewness in these estimates is larger than the ratio of the ion cyclotron frequency at 15 T to the thermal phonon frequency at $T = 15$ K because the elastic constant jump near the defect is assumed to be small in relative terms; skew scattering is larger in relative terms because the reciprocal scattering processes are weak. The sign of the thermal Hall conductivity is negative in many systems—also in agreement with our result (30). It must be noted, however, that the sign of Eq. (30), as well as its magnitude, is very sensitive to the relative strength of elastic and attenuation constants. Both positive and negative signs are possible in our interpretation. When elastic scattering from electrically neutral defects plays a more important role, the κ_H/κ_L (30) ratio should decline. The emergence of an important role for boundary scattering, which normally dominates in the low-temperature limit, is signaled experimentally by a maximum in $\kappa_L(T)$ at a finite temperature $T_{\max}$. The explanation for the phonon Hall effect predicts, in agreement with experiment, that κ_H/κ_L begins to decrease rapidly for $T \ll T_{\max}$.

Discussion. The dominant phonon scattering process in good crystals is generally expected to switch from boundary scattering, to defect scattering, to umklapp phonon-phonon scattering as temperatures increase and typical phonon wavelengths shorten [29,30]. In comparing our theory with experimental data, we must account for these additional scattering processes, which are not expected to be strongly nonreciprocal. If we assume that the heat capacity has its asymptotic T^3 form over the temperature range of interest, we find by applying Mattheisen's rule [29] to phonon scattering that

$$\kappa_L = \frac{AT^3}{C_b + C_dT^4 + C_uT^3\exp(-T^*/T)}, \qquad (31)$$

$$\frac{\kappa_H}{\kappa_L} = \frac{\Lambda_\omega C_dT^4}{C_b + C_dT^4 + C_uT^3\exp(-T^*/T)}. \qquad (32)$$

The constants C_b, C_d, and C_u parametrize the strengths of boundary, defect, and umklapp phonon-phonon scattering, respectively, and are multiplied by characteristic temperature dependencies and summed to obtain the total phonon scattering rate. Here T^* is the umklapp scattering cutoff temperature [29]. At higher temperatures the phonon Hall conductivity in good crystals is insensitive to disorder or boundaries, and it can in principle be accurately described using *ab initio* methods that capture all relevant microscopic details [52–55]. Where this information is available, it can be used to improve the interpretation.

We have explicitly noted in Eq. (32) that the thermal phonon mean-free path $\ell = c\tau_\omega \propto T^{-4}$ [30,31] when

limited by defect scattering alone because phonon scattering from bulk defects declines when phonon wavelengths exceed defect sizes. We fit Eq. (31) to the experimental κ_L data of Ref. [15]. This fit then fixes κ_H/κ_L, up to a single dimensionless skewness scaling parameter Λ_ω, whose value is close to the maximum value of this ratio.

Figure 1 shows that excellent agreement can be achieved between our model and the experimental data. Our results reveal that defect scattering on charge defects can lead to a substantial κ_{xy}/κ_{xx} even farther away from the temperature regime dominated by Rayleigh scattering, i.e., in the red-shaded region in Fig. 1.

Large thermal Hall conductivity signals have been observed in high-temperature superconductors over a wide range of doping between insulating and overdoped states [1–3]. Since phonon chirality is observed to change continuously, decreasing gradually with increases in doping, it is natural to assume that the same mechanism applies in insulating and pseudogap states. If the phonon Hall effect is indeed due to scattering from charged defects, these would have to retain a local effective charge in the pseudogap state. That is to say that local screening by mobile electronic quasiparticles would have to be imperfect at the thermal phonon timescale, on the length scale of the defect. In cuprates phonon chirality drops upon exiting the pseudogap state, which is consistent with

strengthening screening. Note that the Lorentz force on an ion in a doped ionic crystal vanishes only if ionic charges are perfectly screened locally, a condition that is approached only in good metals.

In summary, we have constructed a model of thermal transport by chiral phonons. The phonon conductivity is limited by scattering from charged defects. In our model long-wavelength acoustic phonons experience both elastic and Lorentz force, due to the unscreened charge of the bound dopants. We have shown that the puzzling giant thermal Hall signal observed recently in many dielectric oxides can be explained by the interference between elastic and Lorentz acoustic potentials. The estimated magnitude and sign of the effect is consistent with the low-temperature experimental observations [1–3]. Kinetic viscosity in the crystal is required to get a thermal Hall effect that is linear in field. Future studies should address more systematically the parameters describing the elastic properties of oxygen vacancies as well as their effective charge in insulating and pseudogap phases. We hope that our work will stimulate further experimental investigations of the role of charged defects in phonon-driven thermal transport.

[1] G. Grissonnanche, A. Legros, S. Badoux, E. Lefrancois, V. Zatko, M. Lizaire, F. Laliberté, A. Gourgout, J. Zhou, S. Pyon, T. Takayama, H. Takagi, S. Ono, N. Doiron-Leyraud, and L. Taillefer, Nature (London) **571**, 376 (2019).

[2] M.-E. Boulanger, G. Grissonnanche, S. Badoux, A. Allaire, E. Lefrançois, A. Legros, A. Gourgout, M. Dion, C. H. Wang, X. H. Chen, R. Liang, W. N. Hardy, D. A. Bonn, and Louis Taillefer, Nat. Commun. **11**, 5325 (2020).

[3] G. Grissonnanche, S. Theriault, A. Gourgout, M.-E. Boulanger, E. Lefrancois, A. Ataei, F. Laliberté, M. Dion, J.-S. Zhou, S. Pyon, T. Takayama, H. Takagi, N. Doiron-Leyraud, and L. Taillefer, Nat. Phys. **16**, 1108 (2020).

[4] X. Li, B. Fauqué, Z. Zhu, and K. Behnia, Phys. Rev. Lett. **124**, 105901 (2020).

[5] Y. Kasahara, K. Sugii, T. Ohnishi, M. Shimozawa, M. Yamashita, N. Kurita, H. Tanaka, J. Nasu, Y. Motome, T. Shibauchi, and Y. Matsuda, Phys. Rev. Lett. **120**, 217205 (2018).

[6] L. Zhang, J. Ren, J.-S. Wang, and B. Li, Phys. Rev. Lett. **105**, 225901 (2010).

[7] L. Zhang, J. Ren, J.-S. Wang, and B. Li, J. Phys.: Condens. Matter **23**, 305402 (2011).

[8] M. Mori, A. Spencer-Smith, O. P. Sushkov, and S. Maekawa, Phys. Rev. Lett. **113**, 265901 (2014).

[9] R. Samajdar, S. Chatterjee, S. Sachdev, and M. S. Scheurer, Phys. Rev. B **99**, 165126 (2019).

[10] R. Samajdar, M. S. Scheurer, S. Chatterjee, H. Guo, C. Xu, and S. Sachdev, Nat. Phys. **15**, 1290 (2019).

[11] J. H. Han, J.-H. Park, and P. A. Lee, Phys. Rev. B **99**, 205157 (2019).

[12] J.-Y. Chen, S. A. Kivelson, and X.-Q. Sun, Phys. Rev. Lett. **124**, 167601 (2020).

[13] H. Lee, J. H. Han, and P. A. Lee, Phys. Rev. B **91**, 125413 (2015).

[14] J. Nasu, J. Yoshitake, and Y. Motome, Phys. Rev. Lett. **119**, 127204 (2017).

[15] L. Chen, M.-E. Boulanger, Z.-C. Wang, F. Tafti, and L. Taillefer, arXiv:2110.13277.

[16] R. Hentrich, M. Roslova, A. Isaeva, T. Doert, W. Brenig, B. Buchner, and C. Hess, Phys. Rev. B **99**, 085136 (2019).

[17] Y. Kasahara, T. Ohnishi, N. Kurita, H. Tanaka, J. Nasu, Y. Motome, T. Shibauchi, and Y. Matsuda, Nature (London) **559**, 227 (2018).

[18] M. Hirschberger, J. W. Krizan, R. J. Cava, and N. P. Ong, Science **348**, 106 (2015).

[19] M. Ye, L. Savary, and L. Balents, arXiv:2103.04223.

[20] H. Guo and S. Sachdev, Phys. Rev. B **103**, 205115 (2021).

[21] Y. Onose, T. Ideue, H. Katsura, Y. Shiomi, N. Nagaosa, and Y. Tokura, Science **329**, 297 (2010).

[22] T. Ideue, Y. Onose, H. Katsura, Y. Shiomi, S. Ishiwata, N. Nagaosa, and Y. Tokura, Phys. Rev. B **85**, 134411 (2012).

[23] R. Matsumoto and S. Murakami, Phys. Rev. Lett. **106**, 197202 (2011).

[24] R. Matsumoto and S. Murakami, Phys. Rev. B **84**, 184406 (2011).

[25] P. Laurell and G. A. Fiete, Phys. Rev. Lett. **118**, 177201 (2017).

[26] X. Zhang, Y. Zhang, S. Okamoto, and D. Xiao, Phys. Rev. Lett. **123**, 167202 (2019).

[27] M. Barkeshli, S. B. Chung, and X.-L. Qi, Phys. Rev. B **85**, 245107 (2012).

[28] B. Flebus and A. H. MacDonald, arXiv:2205.13666 (2022).

[29] J. Callaway, Phys. Rev. **113**, 1046 (1959).

[30] P. G. Klemens, Proc. R. Soc. London, Ser. A **208**, 108 (1951).

[31] I. Pomeranchuk, Phys. Rev. **60**, 820 (1941).

[32] M. Levy, M. Xu, B. K. Sarma, and K. J. Sun, in *Physical Acoustics*, Vol. XX, Ultrasonics of High-*T_c* and Other Unconventional Superconductors, edited by M. Levy (Academic Press, New York, 1992), p. 295.

[33] C. Lupien, W. A. MacFarlane, C. Proust, L. Taillefer, Z. Q. Mao, and Y. Maeno, Phys. Rev. Lett. **86**, 5986 (2001).

[34] A. V. Shtyk and M. V. Feigelman, Phys. Rev. B **96**, 064523 (2017).

[35] D. P. Almond, Q. Wang, J. Freestone, E. F. Lambson, B. Chapman, and G. A. Saunders, J. Phys.: Condens. Matter **1**, 6853 (1989).

[36] F. Cordero, Phys. Rev. B **76**, 172106 (2007).

[37] A. M. Bolon, Effect of dopant size on anelastic relaxation in solid state ionics with fluorite structure, Ph.D. dissertation, Texas A&M, 2016.

[38] A. S. Nowick and B. S. Berry, *Anelastic Relaxation in Crystalline Solids* (Academic Press, New York, 1972).

[39] V. M. Ayres and G. C. Gaunaurd, J. Acoust. Soc. Am. **81**, 301 (1987).

[40] Note that this is an arbitrary choice and in principle every direction should be accounted for.

[41] A. C. F. Ying and R. Truell, J. Appl. Phys. **27**, 1086 (1956).

[42] Y. H. Pao and C. C. Mow, J. Appl. Phys. **34**, 493 (1963).

[43] N. G. Einspruch, G. Einspruch, E. J. Witterholt, and R. Truell, J. Appl. Phys. **31**, 806 (1960).

[44] N. G. Einspruch, G. Einspruch, and R. Truell, J. Acoust. Soc. Am. **32**, 214 (1960).

[45] A. D. Brill, G. Gaunaurd, and H. Überall, J. Acoust. Soc. Am. **67**, 414 (1980).

[46] M. K. Hinders, Nuovo Cimento B **106**, 799 (1991); Phys. Rev. A **43**, 5628 (1991).

[47] There is an additional transverse (horizontal shear) wave solution. However, the horizontal shear components are not included in our discussion because they are not excited by an incident compressional wave.

[48] A. D. Pierce, *Acoustics. An Introduction to its Physical Principles and Applications*, 3rd ed. (AIP, New York, 1994), pp. 424–507.

[49] M. Bornm and E. Wolf, *Principles of Optics* (Pergamon Press, New York, 1926).

[50] E. N. Economou, *Green's Functions in Quantum Physics* (Springer-Verlag, Berlin, 1983); E. Merzbacher, *Quantum Mechanics* (John Wiley and Sons Ltd., New York, 1961).

[51] F. Gunkel, D. V. Christensen, Y. Z. Chen, and N. Pryds, Appl. Phys. Lett. **116**, 120505 (2020).

[52] F. Giustino, Rev. Mod. Phys. **89**, 015003 (2017).

[53] D. A. Broido, Appl. Phys. Lett. **91**, 231922 (2007).

[54] A. Ward, D. A. Broido, Derek A. Stewart, and G. Deinzer, Phys. Rev. B **80**, 125203 (2009).

[55] L. Lindsay, A. Katre, A. Cepellotti, and N. Mingo, J. Appl. Phys. **126**, 050902 (2019).